Symmetrical Negative Differential Resistance Behavior of a Resistive Switching Device

Yuanmin Du,[†,*] Hui Pan,[‡] Shijie Wang,[§,*] Tom Wu,[⊥] Yuan Ping Feng,[†] Jisheng Pan,[§] and Andrew Thye Shen Wee[†,*]

[†]Department of Physics, National University of Singapore, 2 Science Drive 3, Singapore 117542, Singapore, [‡]Institute of High Performance Computing, A*STAR (Agency for Science, Technology and Research), 1 Fusionopolis Way, Singapore 138632, Singapore, [§]Institute of Materials Research and Engineering, A*STAR (Agency for Science, Technology and Research), 3 Research Link, Singapore 117602, Singapore, and [⊥]Division of Physics and Applied Physics, School of Physical and Mathematical Sciences, Nanyang Technological University, Singapore 637371, Singapore

ABSTRACT

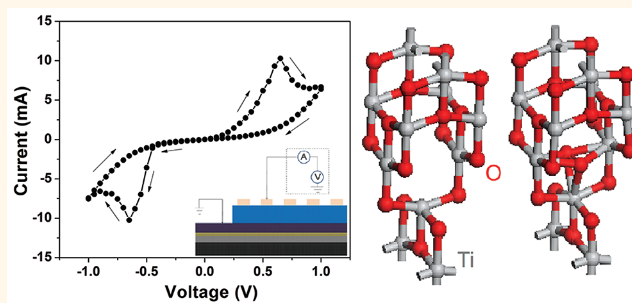

With a thin insulator sandwiched between two electrodes, the negative differential resistance (NDR) behavior has been frequently reported for its potential device applications. Here we report the experimental observation of a symmetric NDR characteristic in a resistive switching device based on TiO_2. We propose a charge storage mechanism for the NDR effect, with oxygen molecular ions working as the active source, in a thin insulating layer. Current–voltage measurements demonstrated a highly reproducible state at about 0.65 eV, and the photoelectron spectroscopy measurements showed that it complies well with the Ti3d band gap state. Our first-principle calculations confirm that charge storage and release arise from trapping and detrapping of oxygen molecular ions at the defect sites. The results and mechanism demonstrated here in a thin layer could be extended to other systems approaching molecular dimensions for device applications.

KEYWORDS: negative differential resistance · charge storage · titanium dioxide · band gap state · oxygen molecular ions · resistive switching

As a well-known concept in device physics, the negative differential resistance (NDR) characteristic has been found in many physical systems such as double quantum wells,[1] superlattices,[2] and one-dimensional systems.[3−8] More than 40 years ago, Simmons and Verderber (SV)[9] proposed a charge storage mechanism to explain the NDR behavior in a MIM structure with a silicon monoxide layer sandwiched between two electrodes. They described that the electroforming process moves gold atoms from the electrode into the SiO layer where an impurity band acting as the electron-trapping states is formed. In 2004, Bozano[4] *et al.* utilized this mechanism to explain the NDR phenomenon in the devices with organic structures as the insulator layer. The space-charge field due to the stored charges at the trapping sites reduces the current through the junction, and the low and high resistance states are obtained. With increasing interest[10−17] in resistance switching effect in the recent years, the charge storage mechanism described by SV has attracted great attention. However, due to the lack of direct evidence from the experiments, the charge storage mechanism is still a subject of debate.[4,5,15] One outstanding challenge is a proper description of the introduced trapping states. The difficulty lies in the *in situ* characterization of the active region for charge storage.

Using metal oxides,[12,13,16−26] organic/polymeric compounds,[4,5,14,15] or nanoparticle assemblies[27] sandwiched between two metal electrodes, the resistive random access memory (ReRAM) has merits such as low power consumption, high speed operation, and high density integration. Various driving mechanisms, including electro-migration of oxygen ions,[18−20] charge trapping,[4,5,9,16,21,28] filamentary conducting,[22−26] and others,[10,11,13] have been suggested to explain the underlying phenomena. Nevertheless, since resistive switching is basically an electrical phenomenon, the current–voltage (I–V) characteristics are essential in deciphering the mechanisms involved. Using passive circuit elements such as resistors, capacitors, and inductors, a memristor model has been proposed.[12,29,30] One of its typical characteristics is the symmetrical I–V

* Address correspondence to yuanmin@nus.edu.sg, sj-wang@imre.a-star.edu.sg, phyweets@nus.edu.sg.

Received for review December 15, 2011 and accepted February 6, 2012.

Published online February 06, 2012
10.1021/nn204907t

©2012 American Chemical Society

behavior, which can be explained by a circuit with two diodes back-to-back.[12] Alternatively, electron tunneling through a thin barrier can also describe this *I*−*V* characteristic.

In this study, we report a resistive switching device with highly reproducible symmetrical NDR characteristic by using a TiO_2 layer sandwiched between two electrodes. Photoelectron spectroscopy experiments are carried out to determine the band gap state. To reveal the charge storage mechanism, first-principles calculations are also performed. We propose that the symmetrical NDR phenomenon comes from an interface insulator layer approaching molecular dimensions. In the electron-tunneling regime, a resistive switching model based on charge trapping and detrapping at a band gap state introduced by oxygen vacancies, with oxygen molecular ions as the active source in charge storage, is presented.

RESULTS AND DISCUSSION

Device Fabrication and Characterization. The amorphous TiO_2 film was deposited on a $Pt/Ti/SiO_2/Si$ substrate by sputter deposition. TiN top electrode (TE) was fabricated using a shadow mask. Figure 1a shows the schematic structure of the device and the *I*−*V* setup. The resistive switching behavior was measured by applying a bias voltage on the TE and with the bottom electrode (BE) grounded. After the electroforming process, a three-phase switching behavior with high repeatability was observed through a voltage sweep between −1.0 and 1.0 V (Figure 1b). The voltage sweep was at 50 mV/step. As the applied voltage increased, the *I*−*V* trace of the device followed an exponential control function. When the voltage reached a certain value (∼0.65 V), the current began to drop, showing a NDR characteristic. The resistance state was translated from a low resistance state to a high resistance state. Then with the decrease of voltage, the *I*−*V* trace followed another exponential control function. As the voltage increased again under a negative voltage polarity, a sudden current jump (occurring randomly between −0.30 and −0.55 V, centered at around 0.40 V) took place before another NDR process (∼−0.65 V).

The exponential *I*−*V* characteristic indicates electron tunneling, and the NDR characteristic on the positive side can be well explained by the charge storage mechanism,[9] where the charge trapping at a specific band gap state is attributed to the NDR behavior in a resistive switching device. To identify such a state, ultraviolet photoemission spectroscopy (UPS) experiments were carried out on the amorphous TiO_2 thin film.

In the stoichiometric form, TiO_2 is a wide band gap insulator, which can be made semiconducting *via* a reduction process. For a single-crystal sample, the sample preparation procedure comprises Ar^+ ion

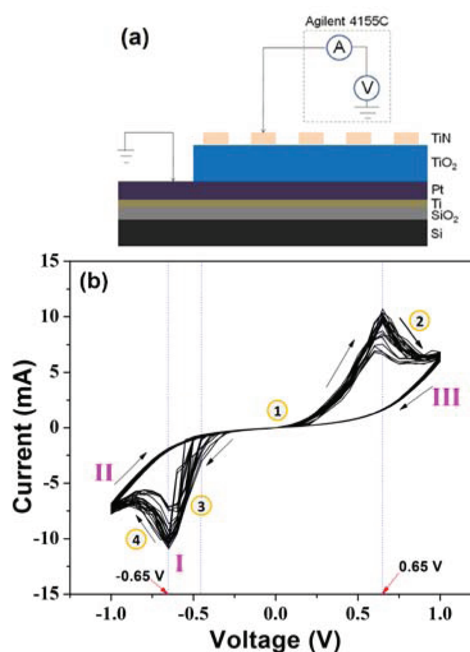

Figure 1. (a) Schematic diagram of the device structure and the *I*−*V* measurement system. (b) Experimental switching *I*−*V* curves. The curves represent 50 experimental switching loops, which show a high degree of repeatability. Phases I, II, and III are defined as the resistance states from the lowest to the highest, respectively. The four circled numbers refer to the sweep stage at different voltages.

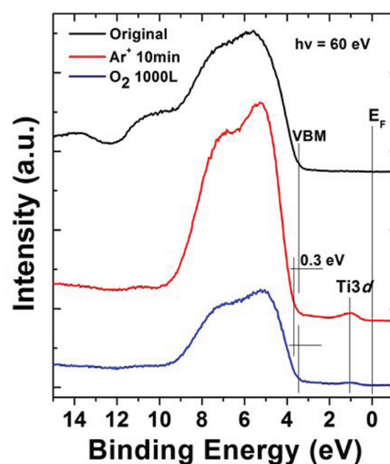

Figure 2. Photoelectron spectroscopy valence band spectra. The as-deposited TiO_2 sample (black) was followed by 10 min Ar^+ ion sputtering (red) and 1000 L oxygen exposure (blue) subsequently.

sputtering and high-temperature annealing prior to UPS measurement.[31,32] The sample structure $TiO_2/Pt/Ti/SiO_2/Si$ in this experiment was prepared through an identical process prior to the deposition of the TiN top electrodes, with the 20 nm TiO_2 top layer deposited under the same conditions as the MIM device structures. The top thin film shows good conductivity and can be used for UPS measurements directly. Figure 2 shows spectra corresponding to the sample without any treatment, after Ar^+ ion sputtering and after an

O_2 exposure of 1000 Langmuirs (L 1L = 1 × 10^{-6} Torr·s). All of the experiments were performed at room temperature.

For the original sample, no band gap state was detected. A ~3.4 eV wide band gap was determined from the measurement. After the sample was sputtered with 500 eV Ar^+ ion for 10 min, a band gap state at ~1.02 eV below the Fermi level was detected. This is consistent with the studies for single-crystal samples based on electron energy loss spectroscopy (EELS)[33] and UPS[32] measurements, with the gap feature observed at ~0.85 eV below the conduction band (CB), which is known as the Ti3d state.[31−33] The Fermi level position is close to the CB. The valence band maximum (VBM) is shifted by ~0.3 eV away from the Fermi level, with respect to the original sample. After an O_2 exposure of 1000 L, the intensity of the Ti3d state decreases dramatically, leaving a residual intensity. There is little change of Ti3d position between the sample after sputtering and after O_2 exposure. At the same time, the VBM position shifts back to that of the original sample after oxygen exposure (Figure 2). For the original sample, the failure to detect the Ti3d state might be due to the low defect concentration, under detection limit of UPS. The two common defects in TiO_2, oxygen vacancy[31] and Ti interstitial,[32] are the two possible origins of the Ti3d state, which has been discussed extensively in recent years.

For an n-type semiconductor, electrons are elevated from a shallow donor level into the CB after an effective doping process. The n-type origin for reduced TiO_2 is still under debate.[34−36] A reduction process for single-crystal TiO_2 creates large amounts of oxygen vacancies and Ti interstitials at the same time. As a comparison to the variable n-type sources under discussion, conducting nanofilaments inside amorphous TiO_2 films could also be the source of the good conductivity. Kwon[22] *et al.* recently reported direct identification of electroformed conducting nanofilaments with oxygen-deficient Magnéli phases inside TiO_2 films for the resistive switching devices. For the Magnéli phase, a work function of ~4.2 eV has been reported,[21] which is close to the electron affinity of TiO_2. Comparably, using density functional theory, a microscopic model for electrically active filaments composed of metallic nickel atoms chains was presented by Lee[24] *et al.*, based on oxygen-deficient NiO structures. Studies on oxide-coated cathode have been started for a long time. From the literature review by Dearnaley,[37] Mutter[38] studied emission and conductivity of such structure and revealed that the oxide conductivity is Ohmic and independent of the current flow direction. As the model proposed by Dearnaley[39] *et al.*, it is supposed that conducting filaments with molecular dimensions are developed through oxide coating. Extended into the oxide matrix, the filaments are directly responsible for the electrical conductivity and the high thermionic emission of the oxide. On the basis of the filamentary theory by Dearnaley *et al.*, a model to explain the observed electrical phenomenon is shown in Figure 3b. Distinct from the host matrix of the oxide, the filamentary conducting paths work as a bridge between the two electrodes. The insulating TiO_2 layer lies at the interface between TE and the bulk oxide layer. During the electroforming process of the devices, a linear $I-V$ characteristic attributed to filamentary conduction has been observed.[40] TiN is widely used as a "diffusion barrier" in semiconductor manufacturing. Under an electro-migration process, oxygen ions tend to pile up at the TE/oxide interface and migrate out through BE. At the top interface, oxidation of the filaments may take place. As a result, a thin interface insulating layer is formed. Electrons need to tunnel through the interfacial layer with filaments as the conducting bridges. As a comparison to the top interface, the TiO_2/Pt(BE) interface acts as an Ohmic contact.[41−43]

On the basis of the Wentzel−Kramers−Brillouin (WKB) approximation, tunneling currents in the direct tunneling regime can be described by the Simmons model (1963).[44,45]

$$J = \frac{e}{2\pi h d^2}\left\{\left(e\varphi_0 - \frac{eV}{2}\right) \times \exp\left[-\frac{4\pi d}{h}(2m)^{1/2}\alpha\left(e\varphi_0 - \frac{eV}{2}\right)^{1/2}\right] - \left(e\varphi_0 + \frac{eV}{2}\right) \times \exp\left[-\frac{4\pi d}{h}(2m)^{1/2}\alpha\left(e\varphi_0 + \frac{eV}{2}\right)^{1/2}\right]\right\} \quad (1)$$

This equation expresses current density as a function of voltage V, with barrier height φ_0 and insulator thickness d being the key parameters that affect the electron direct tunneling through a barrier; h is Planck's constant, α is a unitless parameter[45,46] used for fitting, m is the rest mass of electron, and e is the elementary charge. On the basis of expression 1, a good fit between experiment data and Simmons' model has been obtained, as shown in Figure 3c. Using this method, the interfacial layer thickness was estimated to be 1.84 nm, with the barrier height and the α parameter at 1.04 eV and 0.98, respectively. The data were sampled from the $I-V$ curves of the device shown in Figure 1b.

In the UPS measurements, the Fermi level was moved up to be close to the CB, as a comparison to that of an insulator oxide. On the basis of further analysis of the observed phenomenon, we attribute the 1.02 eV Ti3d state to oxygen vacancies. There has been considerable discussion in the literature about the n-type source for TiO_2. In particular, hydrogen (a ubiquitous impurity in many oxides) has been reported[35,36] to produce shallow donor electrons below the CB. Ti interstitial could be another n-type

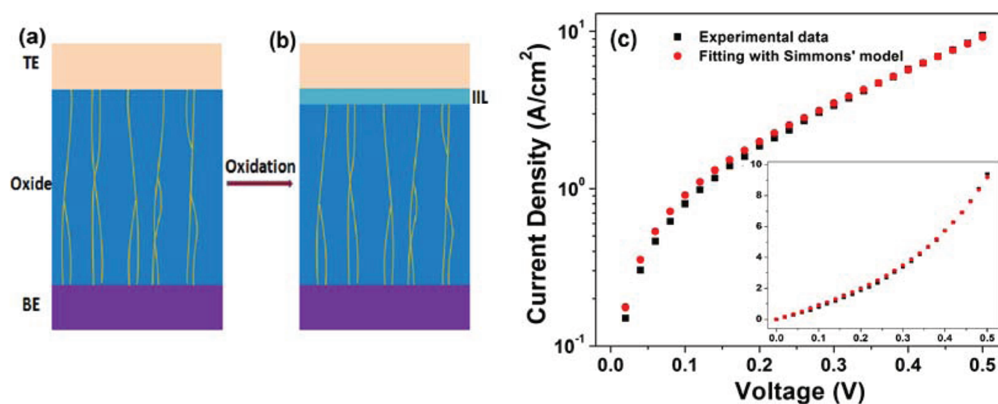

Figure 3. (a,b) Sketch of the model: the top interface is an interface insulating layer (IIL) formed after an oxidation process of the conducting filaments at the interface area; the bulk oxide consists of a number of conducting filaments, as a comparison to the surrounding insulator matrix. (c) Plots of average current density *versus* voltage in a semilog scale: black dotted line shows the raw data sampled from the *I*−*V* curves, and the red dotted line shows the fitting results based on the current tunneling model by Simmons. The inset shows the same curves in a linear scale. The IIL thickness is fitted at ∼1.84 nm.

source for TiO_2. This report is too short to discuss the alternatives in any detail. With TiO_2 as an insulator and the Fermi level in the middle of the band gap, the 0.65 eV state coincides well with that of the 1.02 eV Ti3d state observed in the band gap. The sum of 1.67 eV is very close to the half band gap value of 1.7 eV based on the UPS experiments.

The interface insulator layer comes from the oxidation of the filaments at the top interface and acts as the primary area for charge trapping. With electrons trapping at the band gap state introduced by native oxygen vacancies, the NDR characteristic on the positive side occurs.

First-Principles Modeling. Besides charge trapping, a charge detrapping process is necessary for a reversible switching. A sudden current jump at a negative bias around −0.40 V could be attributed to such a process. With charge continuously trapping and detrapping under the electrical field, the two-sided NDR with symmetric characteristic forms. Oxidation and redox reactions at defect sites like oxygen vacancies may take place, due to the electro-migrated oxygen molecular ions at the interface. As a result, a structure with charged oxygen interstitials is proposed.

To provide further insight into the TiO_2-based NDR characteristics, we carried out first-principles calculations to investigate the electronic properties of TiO_2 with oxygen vacancy defects and interstitial negative charged oxygen atoms. The oxygen vacancy (V_O) is created by removing one oxygen atom from the supercell (Figure 4a). The charged oxygen interstitial is realized by putting an O_2^{2-} into the vacancy site (Figure 4b). The optimized structure (Figure 4a) shows that V_O has little effect on the local structure, indicating that V_O is the dominant defect in TiO_2. By inserting O_2^{2-} into the vacancy site, the local structure is slightly distorted (Figure 4b). The Ti−O bond near the defect is extended by 1%. The distance between Ti and interstitial O is about 2.14 Å and about 4% larger than the Ti−O bond. The O−O bond is 1.49 Å, larger than that in an isolated molecule (1.24 Å). The calculated band gap of the pristine TiO_2 is about 2.7 eV[47,48] (Figure 4c). Defect states are formed within the band gap (0.67 eV above the middle of the band gap) by introducing V_O into TiO_2 (Figure 4d). The position of the defect band within the band gap is close to 0.65 eV value obtained from the *I*−*V* curves. With the vacancy site occupied by mobile charged O_2^{2-}, the V_O states disappear and the E_f shifts to CB (Figure 4e). Charge storage is realized by negative charges fixed at the trapped oxygen atoms, and the device resistance state transfers to another level, leading to the NDR effect.

The sudden current jump observed at a negative voltage (Figure 1b) is related to the release of O_2^{2-} from vacancy sites. The energy barrier for the process is calculated from

$$E_b(O_2^{2-}) = E_{tot}(TiO_2 + V_O + O_2^{2-}) - E_{tot}(TiO_2 + V_O) + E(O_2) - 2E_f \quad (2)$$

where E_{tot} (TiO_2 + V_O) is the total energy of the cell containing a vacancy, E_{tot} ($TiO_2 + V_O + O_2^{2-}$) is the total energy of the cell with the vacancy occupied by O_2^{2-}, and $E(O_2)$ is the energy of oxygen molecule and E_f is the Fermi energy. The calculated energy barrier (E_b) is a function of E_f (Figure 4f). For the charged system, the Fermi level shifts into the CB by electron doping after the oxygen molecular ion was introduced into the neutral cell (Figure 4e). Therefore, E_b is about 0.36 eV, consistent with the threshold values (∼−0.40 eV) from the *I*−*V* curves (Figure 1b). The random characteristic of the threshold voltage values may be due to the different oxygen environments at the interface, during each electrical sweep. On the other hand, the modeling is based on a crystalline interface which represents an ideal situation in contrast to the much more complex situation at the metal/oxide device heterostructures.

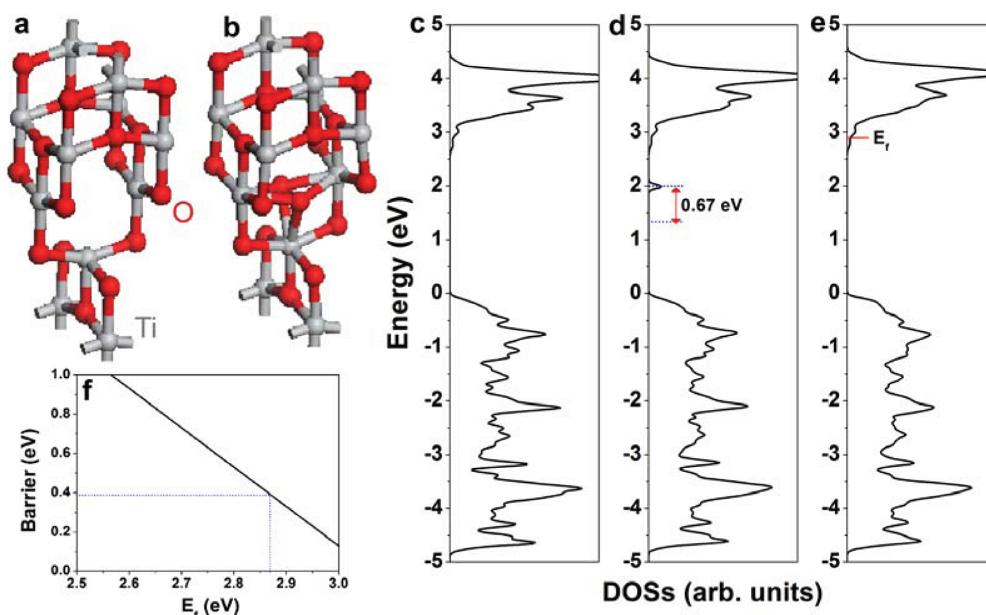

Figure 4. First-principles calculations of TiO_2 with oxygen vacancy and charged oxygen interstitial defects. (a) Local structures of TiO_2 with oxygen vacancy. (b) Local structures of TiO_2 with oxygen vacancy occupied by O_2^{2-}. (c−e) DOSs of TiO_2, TiO_2 with V_O, and TiO_2 with V_O occupied with O_2^{2-}, respectively. (f) Formation energy of oxygen vacancy from the charged oxygen interstitial structure, as a function of the Fermi level (E_f). E_f is measured from the VBM.

Switching Mechanism. With the above analysis, we summarize the resistive switching phenomenon shown in Figure 1b. The different resistance states are defined as phases I, II, and III. (i) With negative charges trapped to one side of the top insulating layer during preceding electroforming processes, the device memory state is at phase II. (ii) With the voltage increasing on the positive side, charges start to be trapped at defect sites on the other side of the insulating layer when V is above 0.65 V. After this stage, the memory state is switched to phase III. (iii) With the voltage under a negative polarity, trapped charges are released from the defect sites (∼−0.40 V), after which the memory state is switched back to phase I. (iv) With further increase of voltage above −0.65 V, negative charges start to be trapped again and the memory state is switched to phase II. With continuous voltage sweeps between −1.0 and 1.0 V, this behavior shows high repeatability. Besides TiN as the TE material, we have also made structures with Pt and Ni as the TE. The symmetric NDR characteristic shown in Figure 1b was only observed for a TiN/TiO_2/Pt structure, due to the difference in oxygen diffusion ability. As a comparison to that of TiN, good oxygen diffusion ability was reported for Pt[49] and Ni.[50] Oxygen molecular ions pile up at the TE/oxide interface under a positive bias and migrate out of the structure through Pt under a negative bias. Under a negative bias, the interface piled oxygen ions tend to be removed, and the temporarily trapped oxygen atoms might be dragged out, upon which oxygen vacancies are then formed.

The interface energy barrier for electrons to tunnel through is changed, due to the piling up of negative charges at the interface. The low and high resistance states are formed, depending on the charge-trapping states at the interface insulator layer. Charges tend to trap from the outer into the inner region of the insulator layer. With oxygen molecular ions trapping into the neutral regions, the Fermi level will be shifted by electron doping, as compared to the other regions of the interface layer without trapped charges. The charge trapping at different regions of the interface insulator oxide is similar to the nonpercolating domain structure,[16] where charge injection and release take place at the specific domains. Moreover, since the negative charges are fixed at the trapped oxygen atoms, it is difficult for the charges to spread through the insulator layer after an electron "traveling" process, according to the theory described by SV.[9]

SV attributed the observed nonvolatile resistance states to electrons trapping to the specific sites introduced by diffusion of gold atoms into the oxide.[9] Instead of using electrons as the source in charge trapping, we interpreted the switching behavior in Figure 1b based on first-principles modeling, by introducing oxygen molecular ions into the TiO_2 cells. Upon microstructure changes, the trapped electrons are fixed at the specific sites. On the other hand, it could also be of a dual process composed of electrons' trapping and a subsequent reaction between oxygen vacancies (with trapped electrons) and nonlattice oxygen molecules. Trapped electrons are fixed with the oxygen atoms at the defect sites of the insulator layer. This leads to using oxygen molecules for charge storage.

CONCLUSION

We have demonstrated symmetrical NDR effects with high repeatability in a resistive switching device. A thin interfacial layer of a few monolayers is attributed as the origin of the observed electrical phenomenon. The oxygen vacancy is proposed as the band gap state and correlated to the Ti3d state. The defect state obtained from the current−voltage curves complies well with that from the photoelectron spectroscopy measurements. The electronic phenomena observed are in agreement with theoretical calculations based on first-principles modeling. In the electron-tunneling regime, with oxygen molecular ions as the active source, a new model based on charge trapping and detrapping is proposed for the observed resistive switching phenomenon. The results suggest that charge storage can be realized by introducing specific defects in a very thin insulating layer. We expect the ability to pattern high repeatability reversible NDR characteristic to present a new direction for high density information storage and processing.

METHODS

Experimental. The 20 nm thick amorphous TiO_2 thin film was deposited on a $Pt/Ti/SiO_2/Si$ substrate by RF magnetron sputtering from a TiO_2 target at room temperature, with Ar gas flow rate at 30 sccm (standard cubic centimeters per minute) and the RF power at 250 W. Circular TiN top electrodes 100 μm in diameter were fabricated by sputtering using a metal shadow mask. The current−voltage measurements of the thin films were carried out at room temperature using an Agilent 4155C semiconductor analyzer. The sample was electroformed by performing $I-V$ sweeps until stable resistive switching behavior was observed. During the electroforming process, the voltage/current level and polarity were the parameters controlled, similar to the report of Jeong *et al.*[19]

The UPS experiments were performed at room temperature, in a UHV end-station (base pressure 1×10^{-10} Torr), at the SINS beamline at the synchrotron radiation facility in SSLS (Singapore Synchrotron Light Source).[51] Valence spectra were acquired with photon energy of 60 eV. E_f was determined by a Fermi edge cutoff from a multilayer Au film. The O_2 exposure was performed at room temperature.

Theoretical. The first-principles calculation based on the density functional theory (DFT)[52] and the Perdew−Burke−Ernzerhof generalized gradient approximation (PBE-GGA)[53] was carried out to find the mechanism. The projector augmented wave (PAW) scheme[54,55] as incorporated in the Vienna *ab initio* simulation package (VASP)[56] was used in the study. The Monkhorst and Pack scheme of k-point sampling was used for integration over the first Brillouin zone.[57] A $3 \times 3 \times 3$ grid for k-point sampling for geometry optimization and an energy cutoff of 380 eV were consistently used in our calculations. The density of states (DOS) have been obtained with a $7 \times 7 \times 7$ mesh. Good convergence was obtained with these parameters, and the total energy was converged to 2.0×10^{-5} eV/atom. The bulk anatase TiO_2 structure (a-TiO_2) is modeled with a $3 \times 3 \times 1$ supercell containing 36 Ti atoms and 72 O atoms. The GGA+U method was used to treat 3d electrons of Ti with the Hubbard on-site Coulomb interaction parameter ($U-J$) to calculate the electronic structures of TiO_2 with and without doping. A value of 5 eV for the $U-J$ is consistently used in our calculations to find the defect level in the band gap comparable with the experimental value.

Conflict of Interest: The authors declare no competing financial interest.

Acknowledgment. This work was supported by MOE Academic Research Fund Grant R398-000-056-112, Singapore. The authors gratefully acknowledge Yee-Chia Yeo for helpful discussions, and Liang Cao for his help with UPS measurements.

REFERENCES AND NOTES

1. Chang, L. L.; Esaki, L.; Tsu, R. Resonant Tunneling in Semiconductor Double Barriers. *Appl. Phys. Lett.* **1974**, *24*, 593–595.
2. Esaki, L.; Chang, L. L. New Transport Phenomenon in a Semiconductor "Superlattice". *Phys. Rev. Lett.* **1974**, *33*, 495–498.
3. Le, J. D.; He, Y.; Hoye, T. R.; Mead, C. C.; Kiehl, R. A. Negative Differential Resistance in a Bilayer Molecular Junction. *Appl. Phys. Lett.* **2003**, *83*, 5518–5520.
4. Bozano, L. D.; Kean, B. W.; Deline, V. R.; Salem, J. R.; Scott, J. C. Mechanism for Bistability in Organic Memory Elements. *Appl. Phys. Lett.* **2004**, *84*, 607–609.
5. Bozano, L. D.; Kean, B. W.; Beinhoff, M.; Carter, K. R.; Rice, P. M.; Scott, J. C. Organic Materials and Thin-Film Structures for Cross-Point Memory Cells Based on Trapping in Metallic Nanoparticles. *Adv. Funct. Mater.* **2005**, *15*, 1933–1939.
6. Zhou, C.; Kong, J.; Yenilmez, E.; Dai, H. Modulated Chemical Doping of Individual Carbon Nanotubes. *Science* **2000**, *290*, 1552–1555.
7. Rakshit, T.; Liang, G.-C.; Ghosh, A. W.; Datta, S. Silicon-Based Molecular Electronics. *Nano Lett.* **2004**, *4*, 1803–1807.
8. Chen, J.; Reed, M. A.; Rawlett, A. M.; Tour, J. M. Large On-Off Ratios and Negative Differential Resistance in a Molecular Electronic Device. *Science* **1999**, *286*, 1550–1552.
9. Simmons, J. G.; Verderber, R. R. New Conduction and Reversible Memory Phenomena in Thin Insulating Films. *Proc. R. Soc. London, Ser. A* **1967**, *301*, 77–102.
10. Waser, R.; Aono, M. Nanoionics-Based Resistive Switching Memories. *Nat. Mater.* **2007**, *6*, 833–840.
11. Waser, R.; Dittman, R.; Staikov, G.; Szot, K. Redox-Based Resistive Switching Memories—Nanoionic Mechanisms, Prospects, and Challenges. *Adv. Mater.* **2009**, *21*, 2632–2663.
12. Yang, J. J.; Pickett, M. D.; Li, X.; Ohlberg, D. A. A.; Stewart, D. R.; Williams, R. S. Memristive Switching Mechanism for Metal/Oxide/Metal Nanodevices. *Nat. Nanotechnol.* **2008**, *3*, 429–433.
13. Sawa, A. Resistive Switching in Transition Metal Oxides. *Mater. Today* **2008**, *11*, 28–36.
14. Scott, J. C.; Bozano, L. D. Nonvolatile Memory Elements Based on Organic Materials. *Adv. Mater.* **2007**, *19*, 1452–1463.
15. Yang, Y.; Ouyang, J.; Ma, L.; Tseng, R. J.-H.; Chu, C.-W. Electrical Switching and Bistability in Organic/Polymeric Thin Films and Memory Devices. *Adv. Funct. Mater.* **2006**, *16*, 1001–1014.
16. Rozenberg, M. J.; Inoue, I. H.; Sànchez, M. J. Nonvolatile Memory with Multilevel Switching: A Basic Model. *Phys. Rev. Lett.* **2004**, *92*, 178302.
17. Lee, M.-J.; Lee, C. B.; Lee, D.; Lee, S. R.; Chang, M.; Hur, J. H.; Kim, Y.-B.; Kim, C.-J.; Seo, D. H.; Seo, S.; *et al.* A Fast, High-Endurance and Scalable Non-volatile Memory Device Made from Asymmetric Ta_2O_{5-x}/TaO_{2-x} Bilayer Structures. *Nat. Mater.* **2011**, *10*, 625–630.
18. Yoshida, C.; Kinoshita, K.; Yamasaki, T.; Sugiyama, Y. Direct Observation of Oxygen Movement during Resistance Switching in NiO/Pt Film. *Appl. Phys. Lett.* **2008**, *93*, 042106.
19. Jeong, D. S.; Schroeder, H.; Breuer, U.; Waser, R. Characteristic Electroforming Behavior in $Pt/TiO_2/Pt$ Resistive Switching Cells Depending on Atmosphere. *J. Appl. Phys.* **2008**, *104*, 123716.
20. Nian, Y. B.; Strozier, J.; Wu, N. J.; Chen, X.; Ignatiev, A. Evidence for an Oxygen Diffusion Model for the Electric

Pulse Induced Resistance Change Effect in Transition-Metal Oxides. *Phys. Rev. Lett.* **2007**, *98*, 146403.
21. Lee, M. H.; Kim, K. M.; Kim, G. H.; Seok, J. Y.; Song, S. J.; Yoon, J. H.; Hwang, C. S. Study on the Electrical Conduction Mechanism of Bipolar Resistive Switching TiO_2 Thin Films Using Impedance Spectroscopy. *Appl. Phys. Lett.* **2010**, *96*, 152909.
22. Kwon, D.-H.; Kim, K. M.; Jang, J. H.; Jeon, J. M.; Lee, M. H.; Kim, G. H.; Li, X.-S.; Park, G.-S.; Lee, B.; Han, S.; *et al.* Atomic Structure of Conducting Nanofilaments in TiO_2 Resistive Switching Memory. *Nat. Nanotechnol.* **2010**, *5*, 148–153.
23. Park, G.-S.; Li, X.-S; Kim, D.-C; Jung, R.-J; Lee, M.-J; Seo, S. Observation of Electric-Field Induced Ni Filament Channels in Polycrystalline NiO_x Film. *Appl. Phys. Lett.* **2007**, *91*, 222103.
24. Lee, H. D.; Magyari-Köpe, B.; Nishi, Y. Model of Metallic Filament Formation and Rupture in NiO for Unipolar Switching. *Phys. Rev. B* **2010**, *81*, 193202.
25. Busani, T.; Devine, R. A. B. Nonvolatile Memory and Anti-fuse Behavior in Pt/a-TiO_2/Ag Structures. *J. Vac. Sci. Technol. B* **2008**, *26*, 1817–1820.
26. Prada, S.; Rosa, M.; Giordano, L.; Di Valentin, C.; Pacchioni, G. Density Functional Theory Study of TiO_2/Ag Interfaces and Their Role in Memristor Devices. *Phys. Rev. B* **2011**, *83*, 245314.
27. Kim, T. H.; Jang, E. Y.; Lee, N. J.; Choi, D. J.; Lee, K.-J.; Jang, J.-T.; Choi, J.-S.; Moon, S. H.; Cheon, J. Nanoparticle Assemblies as Memristors. *Nano Lett.* **2009**, *9*, 2229–2233.
28. Yao, J.; Jin, Z.; Zhong, L.; Natelson, D.; Tour, J. M. Two-Terminal Nonvolatile Memories Based on Single-Walled Carbon Nanotubes. *ACS Nano* **2009**, *3*, 4122–4126.
29. Chua, L. O. Memristor—The Missing Circuit Element. *IEEE Trans. Circuit Theory* **1971**, *CT-18*, 507–519.
30. Strukov, D. B.; Snider, G. S.; Stewart, D. R.; Williams, R. S. The Missing Memristor Found. *Nature* **2008**, *453*, 80–83.
31. Yim, C. M.; Pang, C. L.; Thornton, G. Oxygen Vacancy Origin of the Surface Band-Gap State of TiO_2 (110). *Phys. Rev. Lett.* **2010**, *104*, 036806.
32. Wendt, S.; Sprunger, P. T.; Lira, E.; Madsen, G. K. H.; Li, Z.; Hansen, J. O.; Matthiesen, J.; Blekinge-Rasmussen, A.; Laegsgaard, E.; Hammer, B.; *et al.* The Role of Interstitial Sites in the Ti3d Defect State in the Band Gap of Titania. *Science* **2008**, *320*, 1755–1759.
33. Epling, W. S.; Peden, C. H. F.; Henderson, M. A.; Diebold, U. Evidence for Oxygen Adatoms on TiO_2 (110) Resulting from O_2 Dissociation at Vacancy Sites. *Surf. Sci.* **1998**, *412−413*, 333–343.
34. Di Valentin, C.; Pacchioni, G.; Selloni, A. Reduced and n-Type Doped TiO_2: Nature of Ti^{3+} Species. *J. Phys. Chem. C* **2009**, *113*, 20543–20552.
35. Panayotov, D. A.; Yates, J. T., Jr. n-Type Doping of TiO_2 with Atomic Hydrogen-Observation of the Production of Conduction Band Electrons by Infrared Spectroscopy. *Chem. Phys. Lett.* **2007**, *436*, 204–208.
36. Finazzi, E.; Di Valentin, C.; Pacchioni, G.; Selloni, A. Excess Electron States in Reduced Bulk Anatase TiO_2: Comparison of Standard GGA, GGA+U, and Hybrid DFT Calculations. *J. Chem. Phys.* **2008**, *129*, 154113.
37. Dearnaley, G. A Theory of the Oxide-Coated Cathode. *Thin Solid Films* **1969**, *3*, 161–174.
38. Mutter, W. E. personal communication quoted by Eisenstein, A. S. Oxide Coated Cathodes. *Adv. Electron. Electron Phys.* **1948**, *1*, 1−64.
39. Dearnaley, G.; Stoneham, A. M.; Morgan, D. V. Electrical Phenomena in Amorphous Oxide Films. *Rep. Prog. Phys.* **1970**, *33*, 1129–1191.
40. The electroforming process plays an important role in determining the current−voltage characteristics.[19] Under an electrical bias, the electro-migration of oxygen ions may result in compositional and structural changes.[18−20] Linear $I-V$ behavior,[19,42] indicating filamentary conductance, has been observed during the electroforming process of the devices.
41. Dwyer, D. J.; Cameron, S. D.; Gland, J. Surface Modification of Platinum by Titanium Dioxide Overlayers: A Case of Simple Site Blocking. *Surf. Sci.* **1985**, *159*, 430–442.
42. Zhong, N.; Shima, H.; Akinaga, H. Rectifying Characteristic of Pt/TiO_x/Metal/Pt Controlled by Electronegativity. *Appl. Phys. Lett.* **2010**, *96*, 042107.
43. Tamura, T.; Ishibashi, S.; Terakura, K.; Weng, H. First-Principles Study of the Rectifying Properties of Pt/TiO_2 Interface. *Phys. Rev. B* **2009**, *80*, 195302.
44. Simmons, J. G. Generalized Formula for Electric Tunnel Effect between Similar Electrodes Separated by a Thin Insulating Film. *J. Appl. Phys.* **1963**, *34*, 1793–1803.
45. Holmlin, R. E.; Haag, R.; Chabinyc, M. L.; Ismagilov, R. F.; Cohen, A. E.; Terfort, A.; Rampi, M. A.; Whitesides, G. M. Electron Transport through Thin Organic Films in Metal−Insulator−Metal Junctions Based on Self-Assembled Monolayers. *J. Am. Chem. Soc.* **2001**, *123*, 5075–5085.
46. Definition of the fitting parameter,[45] α, varies. It might be caused by a nonrectangular barrier shape, the effective mass of the electron tunneling through the barrier, or a combination of both.
47. GGA approach always underestimates the band gap of material. The calculated band gap is ~2.7 eV with the Coulomb interaction parameter ($U-J=5$) used. We do not expect to be able to open up the band gap using any "reasonable" U value,[34,36,48] nor is this our goal here.
48. Hu, Z.; Metiu, H. Choice of U for DFT+U Calculations for Titanium Oxides. *J. Phys. Chem. C* **2011**, *115*, 5841–5845.
49. Matsui, Y.; Suga, M.; Hiratani, M.; Miki, H.; Fujisaki, Y. Oxygen Diffusion in Pt Bottom Electrodes of Ferroelectric Capacitors. *Jpn. J. Appl. Phys.* **1997**, *36*, L1239–L1241.
50. Park, J.-W.; Altstetter, C. J. The Diffusion and Solubility of Oxygen in Solid Nickel. *Metall. Trans. A* **1987**, *18*, 43–50.
51. Yu, X. J.; Wilheimi, O.; Moser, H. O.; Vidyarai, S. V.; Gao, X. Y.; Wee, A. T. S.; Nyunt, T.; Qian, H.; Zheng, H. New Soft X-ray Facility SINS for Surface and Nanoscale Science at SSLS. *J. Electron Spectrosc. Relat. Phenom.* **2005**, *144−147*, 1031–1034.
52. Hohenberg, P.; Kohn, W. Inhomogeneous Electron Gas. *Phys. Rev.* **1964**, *136*, B864–B871.
53. Perdew, J. P.; Burke, K.; Ernzerhof, M. Generalized Gradient Approximation Made Simple. *Phys. Rev. Lett.* **1996**, *77*, 3865–3868.
54. Blöchl, P. E. Projector Augmented-Wave Method. *Phys. Rev. B* **1994**, *50*, 17953–17979.
55. Kresse, G.; Joubert, D. From Ultrasoft Pseudopotentials to the Projector Augmented-Wave Method. *Phys. Rev. B* **1999**, *59*, 1758–1775.
56. Kresse, G.; Furthmüller, J. Efficient Iterative Schemes for *Ab Initio* Total-Energy Calculations Using a Plane-Wave Basis Set. *Phys. Rev. B* **1996**, *54*, 11169–11186.
57. Monkhorst, H. J.; Pack, J. D. Special Points for Brillouin-Zone Integrations. *Phys. Rev. B* **1976**, *13*, 5188–5192.